PERGAMON

Engineering Fracture Mechanics 68 (2001) 1669–1686

Engineering Fracture Mechanics

www.elsevier.com/locate/engfracmech

Mechanism of effects of warm prestressing on apparent toughness of precracked specimens of HSLA steels

J.H. Chen [a,*], V.B. Wang [a], G.Z. Wang [a], X. Chen [b]

[a] *Gansu University of Technology, Lanzhou, Gansu 730050, China*
[b] *Wuhan Iron and Steel Co., Wuhan 430080, China*

Received 10 October 2000; received in revised form 19 February 2001; accepted 30 March 2001

Abstract

In this work, based on the results for: (1) variation of apparent toughness measured at low temperature in precracked HSLA steel specimens which had experienced various cycles of warm prestressing (WPS), (2) detailed observations and measurements of microscopic parameters on fracture surfaces, (3) comprehensive finite element method calculations, the mechanisms for the effects of WPS are analyzed. The effects of blunting of the precrack tip on reducing normal tensile stress by decreasing the stress triaxiality and strain developing in front of the tip are identified as the main factors improving the apparent toughness. The effects of residual compressive stress are separated from that of crack tip blunting and play a secondary role in the improvement of the apparent toughness of steel showing Bauschinger effect. The residual tensile stress is proved to be deleterious to the apparent toughness. © 2001 Elsevier Science Ltd. All rights reserved.

Keywords: Warm prestressing; Fracture toughness; HSLA steel; Critical crack opening displacement specimen; Finite element method calculation

1. Introduction

A great amount of evidence has been accumulated which demonstrates the beneficial effects of warm prestressing (WPS) on improving the apparent fracture toughness of precracked and notched specimens. In a widely cited paper [1], Nichols attributed the beneficial effects to three mechanisms

1. work hardening to prevent yield on reloading;
2. local yield on preload introducing beneficial local stresses;
3. change of shape of the tip of the defect (notch-blunting).

* Corresponding author. Fax: +86-931-2755-806.
E-mail address: zchen@gsut.edu.cn (J.H. Chen).

0013-7944/01/$ - see front matter © 2001 Elsevier Science Ltd. All rights reserved.
PII: S0013-7944(01)00051-0

Nomenclature

a	crack length
B	thickness of specimen
CF	cooling–fracturing cycle
COD	critical crack opening displacement
E	Young's modulus
FEM	finite element method
HSLY	high strength low alloying
K	elastic part of K_{WPS}
K_{WPS}	warm prestress intensity
LCF	loading–cooling–fracturing cycle
LCUF	loading–cooling–unloading–fracturing cycle
LUCF	loading–unloading–cooling–fracturing cycle
LUfLUCF	loading–unloading–inversely loading–cooling–fracturing
P_f	fracture load
P_{gy}	general yield load
P_0	Prestressing load
S	loading span of COD specimen
V_p	plastic displacement of the loading point
W	width of specimen
WPS	warm prestressing
X_f	distance from cleavage origin to blunted crack tip
δ	symbol of crack opening displacement
δ_e	elastic part of δ
δ_p	plastic part of δ
ε_p	plastic strain
v	Poisson's constant
γ_p	hinge factor
σ_{flow}	flow stress
σ_m/σ_e	stress triaxiality
σ_{peak}	maximum value of σ_{yy}
σ_y	yield stress
σ_{yy}	normal principal stress

Harrison and Fearnehough [2] explained the benefit shown by specimens which were fractured without unloading (i.e. without residual compressive stress) from the prestress level by the generation of a large plastic zone at the notch root which modified the stress pattern on testing at low temperature as compared with a virgin specimen. This argument is consistent with item (1) of Nichols.

In a non-monotonic loading process the near-tip elastic–plastic fields are expected to be load-path dependent, such that in general they cannot be uniquely characterized by the J-integral alone. Chell et al. [3] suggested a parameter J_e which evaluates the force on all mobile dislocations enclosed by a contour which separates the plastic and residual zones. The stress distribution at a crack tip subjected to a WPS cycle can be obtained by the superposition of the appropriate monotonic loading stress distributions evaluated by J_e. Curry [4] further combined this model and the cleavage fracture criteria specified by the RKR model [5] to predict the effects of WPS and strain aging.

Recent investigations of Reed and Knott [6–8] emphasized the role of the local residual stress based on the observation that stress-relief heat treatments after prestressing remove nearly all the beneficial effects of WPS. Tensile prestress cycles give rise to residual compressive stress, and then the condition of fracture at low temperature cannot be reached until the effect of the residual stress is eliminated. The effect of notch blunting is ignored by listing the facts that in blunt notch specimen the beneficial effect of WPS remains even when ductile micro-cracks occur at the tip of notches.

But based on the experimental results that the level of unloading from prestressing produced no effect on the improvement of apparent toughness, Timofeev [9] concluded that residual compressive stress is not the main factor improving the apparent toughness though it plays the main role when the prestressing is low. With increasing prestress the effects of crack tip blunting and strain hardening increase and dominate the process. In Chell's model these factors are not involved which results in the deviation of theoretical estimation from experimental results.

But by quantitative investigation of the effects of WPS, Stoeckl et al. [10] reveals that the WPS effect is well correlated with the crack blunting. The latter retards the stress intensification with increasing applied load.

Shum [11] carried out comprehensive FEM calculations to quantitatively describe the path-dependent non-monotonic-loading near-tip crack-tip field. Besides the traditional explanation attributing the WPS effects to the residual compressive stress, the progressive loss of constraint was suggested as an alternative explanation for absence of crack initiation in monotonic loading–cooling process.

Recently, the present authors investigated the mechanism of the effects of WPS on the apparent toughness measured in notched specimens [12]. It is revealed that the effects of tensile warm prestressing on the improvement of the apparent toughness of notched specimens results from three factors, i.e. the residual compressive stress, macroscopic blunting of the original notch, and prestrain-deactivating cleavage initiation. Theses factors are each effective at various extents of prestressing, specified by a prestress ratio defining prestressing load P_0, as a fraction of the general yield load P_{gy}. For values of prestress ratio, P_0/P_{gy}, lower than 1.0, the residual compressive stress acts as the main factor. Between prestress ratio of 1.0 and 1.5 values, in addition to the residual compressive stress the macroscopic blunting of the notch root plays an increasing role. The effect of the prestrain-deactivating cleavage initiation is present at prestress ratios, $P_0/P_{gy} \geqslant 1.2$. In the case of compressive-warm prestressing, the apparent toughness is reduced due to the residual tensile stress.

From the review introduced above it is apparent that the mechanism of WPS effects is still an attractive subject. This paper focuses on identification of the main factors affecting the apparent toughness measured in precracked specimens by analyzing the roles played separately by the macro-blunting of the precrack tip and the residual compressive stress.

2. Experimental

2.1. Material and specimens

2.1.1. Material

A HSLA steel WCF-62 with the composition shown in Table 1 is used. It is provided in the quenched and tempered state. Its microstructure is shown in Fig. 1.

2.1.2. Specimens

Standard COD test specimens and round tensile test specimens with the dimensions shown in Fig. 2(a) and (b) are cut from 45 mm thickness steel plate in the LT direction.

Table 1
Compositions of HSLA steel WCF-62 (wt.%)

C	Si	Mn	Ni	Cr	Mo	V	B	S	P
0.06	0.23	1.36	0.36	0.19	0.21	0.03	0.0017	0.009	0.02

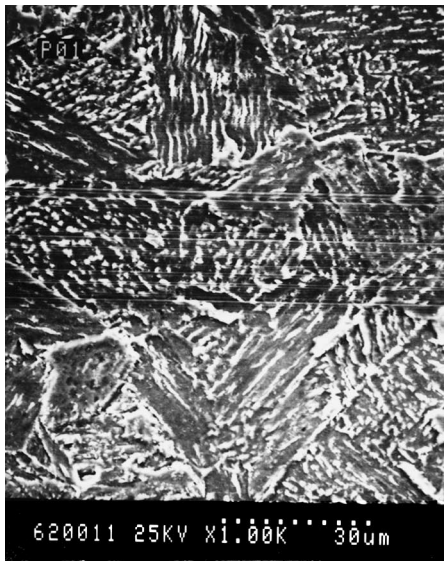

Fig. 1. Microstructure of HSLA steel WCF 62.

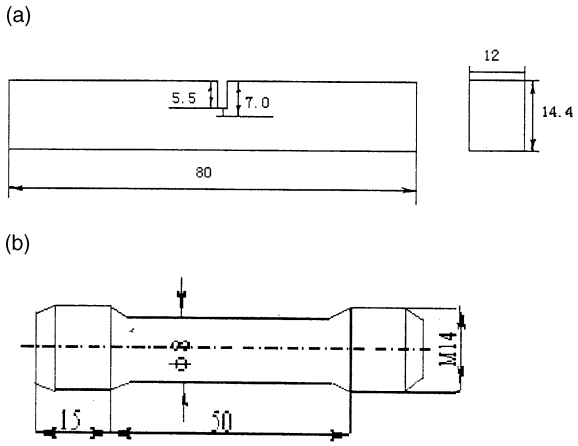

Fig. 2. Dimensions of (a) COD specimens, and (b) tensile test specimens.

2.2. Macroscopic mechanical tests

Tensile tests are carried out on a Shimadzu AG-10TA universal testing machine with a crosshead speed of 1 mm/min at a range of temperature from −196°C to 20°C. Yield stress σ_y and strain hardening exponent n are measured.

The Bauschinger effect of steel WCF-62 is measured by a Mitsubishi low cycle fatigue tester with specimens of the same size as the tensile ones. Three cycles are measured with constant tensile or compressive strain of 0.1 at a crosshead speed of 2 mm/min. The parameters of kinematic hardening model are determined by curve fitting of the first half cycle.

WPS cycles are conducted on a Shimadzu AG-10TA testing machine at 20°C with the fracture steps at −130°C and −196°C. WPS cycles CF, LCF, LUCF, and LCUF, are performed using three point bending COD specimens. Here C, F, L, U, mean cooling, fracturing, loading, and unloading (see Fig. 3).

The values of stress intensity factors exerted by warm prestressing, K_{WPS} and at low temperature fracture, K_f are calculated by the equations:

$$K_{WPS} = P_0 SY(a/W)/BW^{3/2}, \tag{1}$$

$$K_f = P_f SY(a/W)/BW^{3/2}. \tag{2}$$

Here P_0 is the load of prestressing, P_f the fracture load, B the thickness of specimen, W the width of specimen, a the crack length, loading span $S = 4W$ and

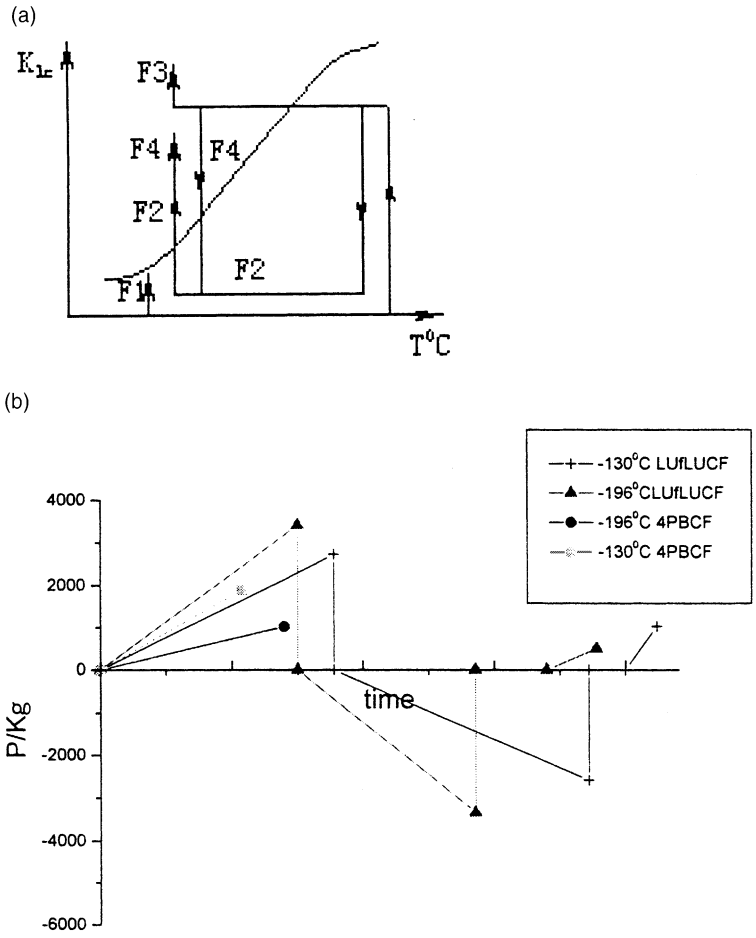

Fig. 3. Various cycles of WPS and fracture: (a) CF(F1), LUCF(F2), LCUF(F4), and LCF(F3) (b) LUfLUCF.

$$Y(a/W) = 2.9(a/W)^{1/2} - 4.6(a/W)^{3/2} + 21.8(a/W)^{5/2} - 37.6(a/W)^{7/2} + 38.7(a/W)^{9/2}. \quad (3)$$

The crack opening displacement produced by WPS δ_{WPS} is calculated by equations:

$$\delta_{WPS} = \delta_e + \delta_p, \quad \delta_e = K^2(1-\nu^2)/2\sigma_y E, \qquad \delta_p = \gamma_p(W-a)V_p/W.$$

Here δ_e is the elastic part, δ_p the plastic part, K the elastic part of K_{WPS}, γ_p the hinge factor taken as 0.45, V_p the plastic displacement of the loading point.

A special cycle named LUfLUCF is used in four-point bending COD specimens. Here fL means bending in an opposite direction to the normal loading which is used after loading and unloading steps to return the blunted precrack tip to its original shape and results in a residual tensile stress in front of it. Fig. 3 schematically shows various WPS and fracture cycles.

2.3. Observation of fracture and metallographic surface

Fracture surfaces are observed in detail by a scanning electron microscope SEM 520. The cleavage initiation position is located by tracing the river pattern strip back to its origin, and the distance X_f from this origin to the blunted crack tip is measured. From the curves calculated by FEM in this work, the normal stress σ_{yy}, stress triaxiality σ_m/σ_e, and plastic strain ε_p at the cleavage origin are obtained and defined as the local fracture stress σ_f critical stress triaxiality T_C and fracture strain ε_{pc} respectively.

The metallographic surface cut perpendicularly to the front of the precrack tip in the specimen unloaded prior to fracture is observed to identify the tip blunting and occurrence of micro-cracks or cavities.

2.4. Finite element method calculations

FEM calculations are performed with the ABAQUS code using a kinematic hardening elastic–plastic model. Fig. 4 shows that eight elements are arranged around the crack tip with an original radius varying from 0.5, 2.0, to 15 μm according to the levels of prestressing. Eight-node biquadratic plain strain hybrid elements with reduced integration (CPE8RH) are used for meshes which experience large strain. Normal eight-node biquadratic plain strain elements (CPE8) are used for the remainder.

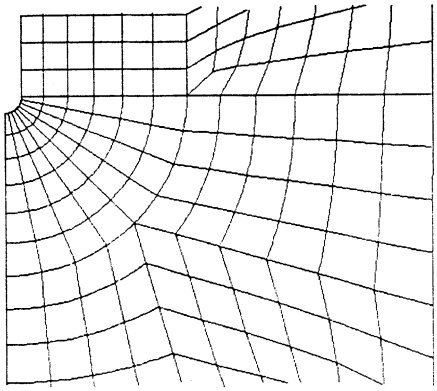

Fig. 4. Arrangement of FEM calculation mesh adjacent to the crack tip.

Table 2
Results of tensile tests

T (°C)	20	−30	−50	−70	−100	−120	−196
σ_y (MPa)	543	582	590	–	655	672	1004
n	0.19	0.21	0.19	0.22	0.24	0.22	0.10

3. Experimental results

3.1. Results of tensile tests

Table 2 shows the results of tensile tests.

3.2. Results of Bauschinger effect measurement

A typical stress–strain curve of the first one and half fatigue cycles measured at 20°C is shown in Fig. 5(a). It identifies the Bauschinger effect with the sum of the tensile and compressive yield strengths equaling 1120 MPa. Fig. 5(b) shows the stress–strain curves used for the kinematic hardening model which are described by the following formulas:

$$\sigma_{\text{flow}} = 600 + 4000(1 - \exp(-7\varepsilon_{\text{p}}))/7 \text{ (MPa)} \quad \text{at } 20^{\circ}\text{C}$$

and

$$\sigma_{\text{flow}} = 1000 + 1000(1 - \exp(-7\varepsilon_{\text{p}}))/7 \text{ (MPa)} \quad \text{at } -196^{\circ}\text{C}.$$

Here ε_{p} the plastic strain and σ_{flow} is the flowing stress.

3.3. Results of apparent toughness of specimens experiencing WPS cycles with various prestressing levels

The results of apparent toughness measurements in specimens experiencing LUCF, LCUF and LCF cycles are summarized in Fig. 6(a)–(c) for fracture at −196°C and Fig. 7(a)–(c) at −130°C. The values of apparent fracture toughness measured at low temperatures are plotted against the levels of prestressing carried out at 20°C. It can be found that the apparent toughness is appreciably improved in specimens fractured at −196°C when the prestressing load reaches general yielding at around 9000 N. The apparent toughness of specimens fractured at −130°C benefit a little from WPS. The LCF cycles produce the highest toughness. The LCUF cycles offer stable and high toughness values compared with those produced by LUCF.

The apparent toughnesses measured in specimens experiencing LUfLUCF cycles are indicated by the ends of the corresponding curves shown in Fig. 3(b). For comparison the values of toughness measured in four-point bending specimens directly fractured at −130°C and −196°C are shown in the same figure. The toughness of specimen experiencing LUfLUCF WPS cycle is apparently lower than that of specimens directly fractured at the same temperature.

3.4. Results of observations on fracture and metallographic surfaces

Fracture surfaces show the cleavage pattern in specimens tested at −196°C (Fig. 8a). In specimens tested at −130°C after WPS narrow regions of fibrous tearing can be found on the fracture surfaces (Fig. 8b). Most cleavage events are triggered at second phase particles as shown in Fig. 9. The distances X_{f} from the cleavage initiation positions to the blunted crack tips are measured. The values of σ_{f}, $\sigma_{\text{m}}/\sigma_{\text{e}}$, and ε_{pc} at X_{f}

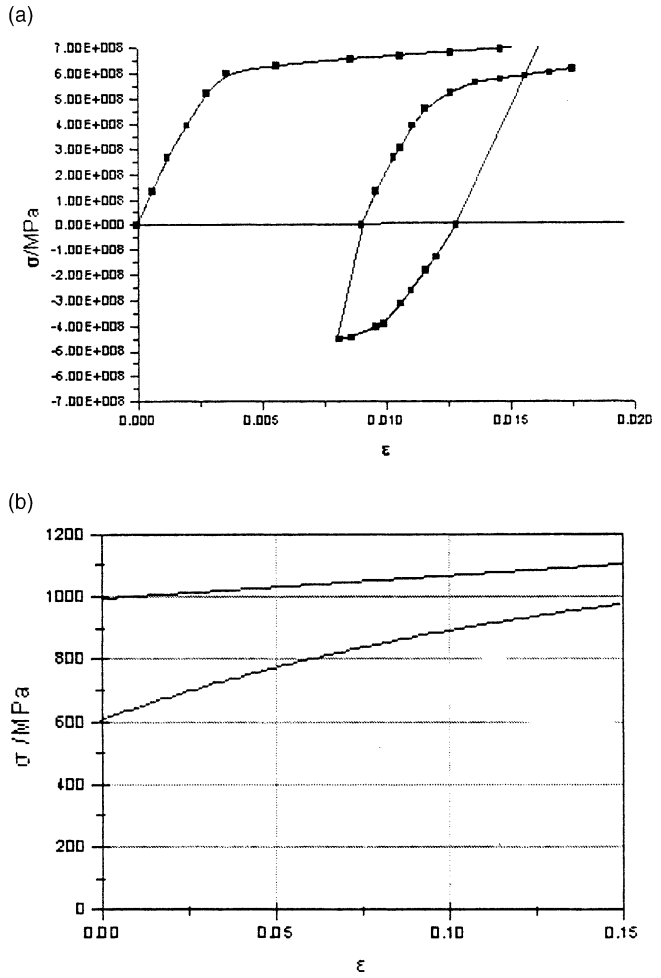

Fig. 5. (a) Stress–strain curve of the first one and half cycle measured at 20°C by low cycle fatigue test and (b) curves for kinematic hardening model upper −196°C, lower 20°C.

are read from the calculated curves of normal stress, stress triaxiality, and strain distribution in front of the blunted crack tip and listed in Tables 3 and 4.

Metallographic sections prepared after prestressing show apparent opening of the original crack tip and in some cases a micro-crack (20–30 μm) emerging from it (Fig. 10(a)). Micro-cavities evolved from second phase particles can be found in the heavily strained vicinity of the blunted crack tip (Fig. 10(b)). These particles cannot be triggered again as cleavage origins.

3.5. Results of FEM calculations

Comprehensive results of FEM calculations of normal stress, stress triaxiality, and plastic strain distributions at every step of various WPS cycles are obtained. Fig. 11 shows typical calculated distributions of normal stress in front of precrack tips at the last fracture step at −196°C. In Fig. 11(a) the normal stress evolves with applied load for a directly fracturing cycle (CF). Fig. 11(b) shows the case for a LUCF cycle

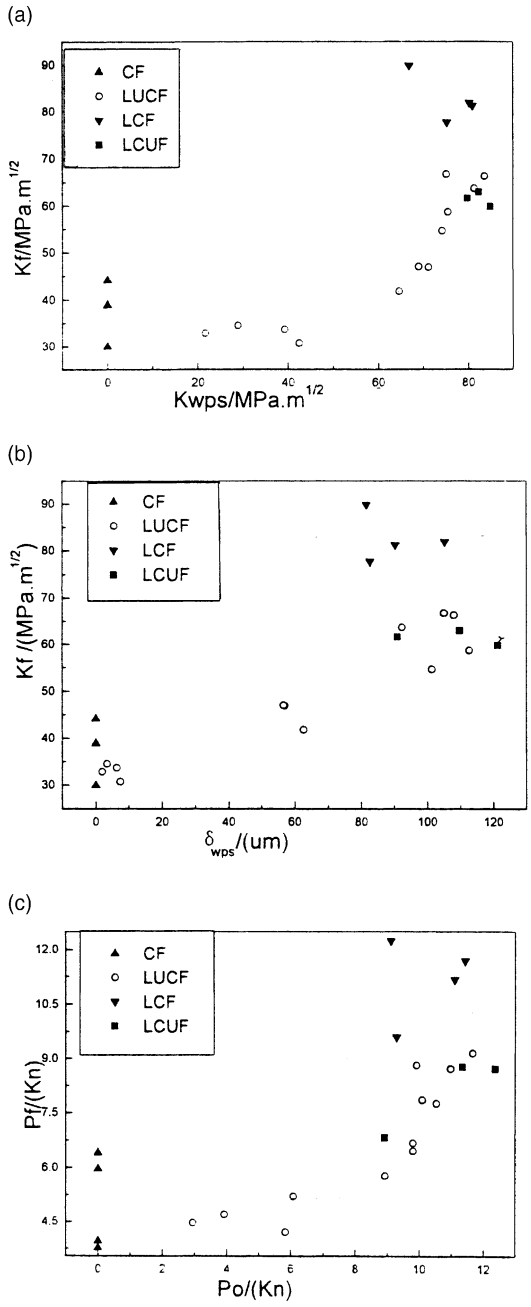

Fig. 6. Parameters associated with apparent fracture toughness measured at −196°C plotted against prestressing level at 20°C: (a) K_f–K_{WPS}, (b) K_f–δ_{WPS}, (c) P_f–P_0.

after a WPS load of 10 kN. In the later case it is found that the compressive normal stress becomes to a tensile stress at a relative low applied load. But the rate of tensile stress increase with the applied load is much lower than in the case of direct fracture. For reaching a peak tensile stress of about 2300 MPa at the

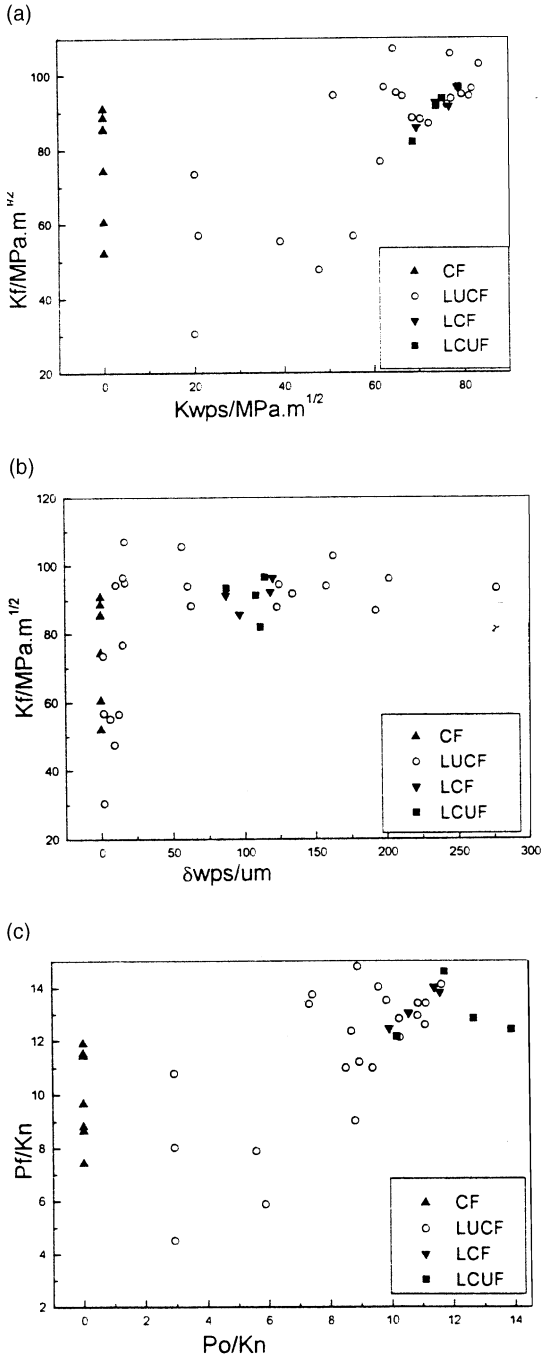

Fig. 7. Parameters associated with apparent fracture toughness measured at −130°C plotted against prestressing level at 20°C: (a) K_f–K_{WPS}, (b) K_f–δ_{WPS}, (c) P_f–P_0.

last step of fracturing a load of 7600 N (Fig. 11(b)) should be applied for a LUCF cycle with 10 kN prestressing, but only 1700 N for a CF cycle (Fig. 11(a)).

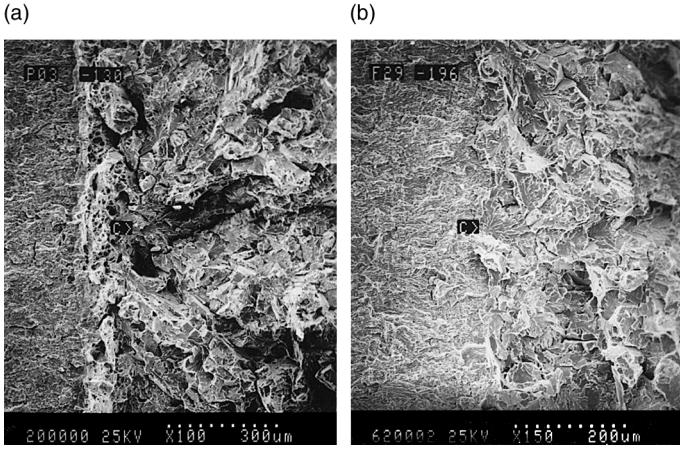

Fig. 8. Typical fracture surface of specimens tested at (a) −130°C (b) −196°C.

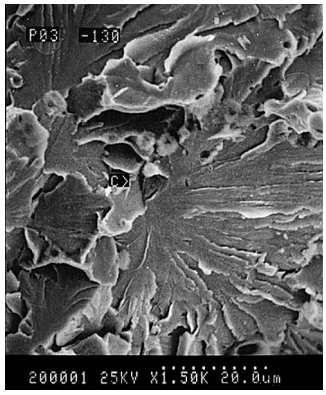

Fig. 9. Cleavage facet initiated at a second phase particle.

Table 3
Fracture-related mechanical parameters produced during LUCF cycle with various prestressing load (fracturing step at −196°C)

	P_0 (N)					
	0	3000	6000	8000	9000	10 200
Produced at the beginning of fracturing step						
U (μm)	0	0.5	1.8	3.9	6.3	45.5
σ_{resmax} (MPa)	0	−1191	−1355	−1407	−1320	−1120
Produced by fracturing load of 5000 N at −196°C						
$\sigma_{yy\,\max}$ (MPa)	2900	2897	2730	2540	2476	2020
ε_{p}	0.022	0.020	0.019	0.015	0.015	0.007
$(\sigma_{\text{m}}/\sigma_{\text{e}})_{\max}$	2.22	2.20	2.00	1.95	1.72	1.35

P_0 is the prestressing load, U the crack opening displacement, σ_{resmax} the peak residual compressive stress, $\sigma_{yy\,\max}$ the peak normal stress, ε_{p} the plastic strain, $(\sigma_{\text{m}}/\sigma_{\text{e}})_{\max}$ the peak stress triaxiality.

Table 4
Fracture-related mechanical parameters produced during LUCF cycle with various prestressing load (fracturing step at −130°C)

	P_0 (N)					
	0	3000	6000	8000	9000	10 080
Produced at the beginning of fracturing step						
U (μm)	0	0.5	1.8	3.9	6.3	43.2
$\sigma_{\text{res max}}$ (MPa)	0	−1191	−1355	−1407	−1320	−1016
Produced by fracturing load of 9500 N at −130°C						
$\sigma_{yy\,\text{max}}$ (MPa)	2420	2400	2386	2320	2205	2008
ε_p	0.063	0.061	0.071	0.059	0.060	0.073
$(\sigma_m/\sigma_e)_{max}$	2.64	2.62	2.55	2.51	2.41	2.20
Measured at the end of fracturing step						
σ_f (MPa)	2236	2255	2175	2350	2333	2136

P_0 is the prestressing load, U the crack opening displacement, σ_{resmax} the peak residual compressive stress, $\sigma_{yy\,\text{max}}$ the peak normal stress, ε_p the plastic strain, $(\sigma_m/\sigma_e)_{max}$ the peak stress triaxiality, σ_f the local fracture stress.

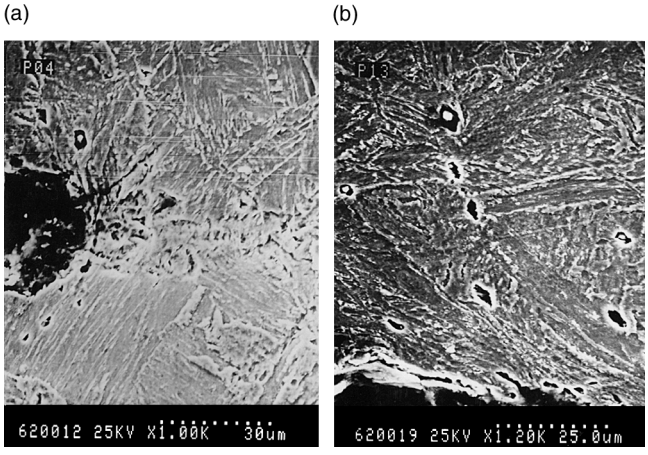

Fig. 10. (a) Metallographic sections showing opening of original crack tip and micro-crack emerging from it and (b) micro-cavities in heavily strained vicinity of blunted crack tip.

4. Discussion

Before discussing the mechanism of the effects of the WPS, it should be pointed out that, as shown by Table 4 and Fig. 13 the local fracture stress σ_f remains almost constant after WPS at various levels. It means that the real toughness of steel is almost unmodified by WPS, the effects of which are apparent only on the apparent toughness of steel specimens.

The effects of prestrain-deactivating cleavage initiation by micro-cavities evolvement will be investigated in future work.

4.1. Effects of crack tip blunting

Table 3 compares the fracture-related mechanical parameters produced by an applied load of 5000 N at −196°C in specimens experiencing various prestressing loads. The load of 5000 N is selected as it is the

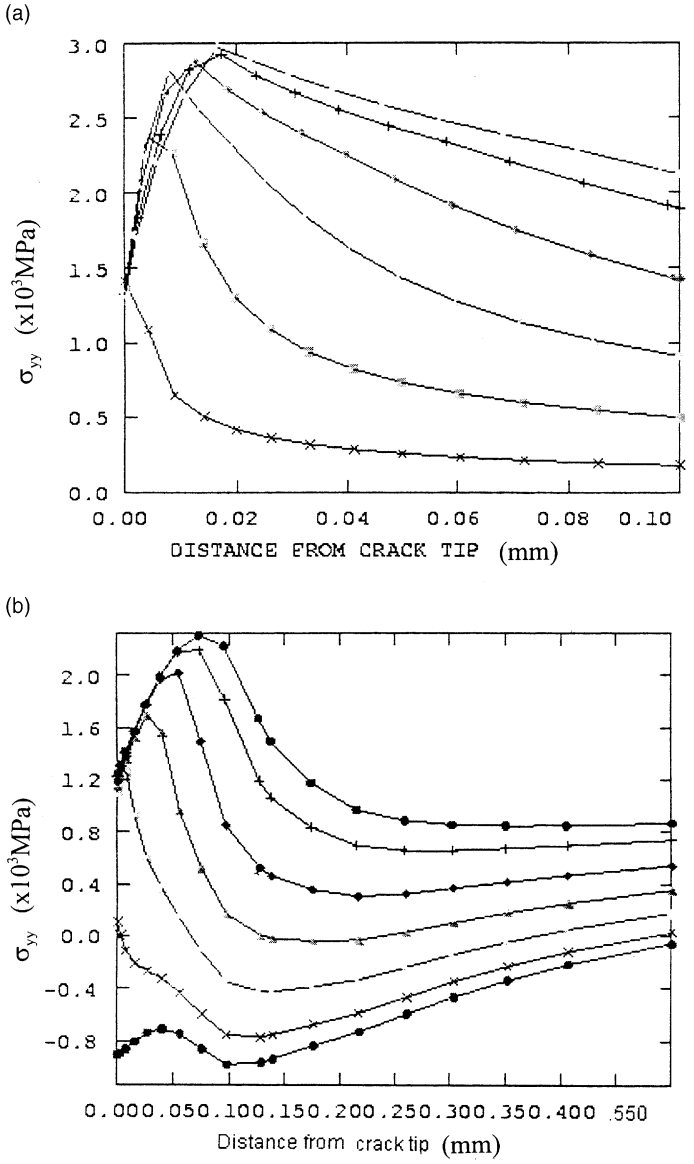

Fig. 11. Calculated normal stress distribution in front of precrack tip at the fracturing step. (a) Directly fracturing at −196°C: (×) $P_f = 642$ N, (■) $P_f = 1765$ N, (▲) $P_f = 3029$ N, (♦) $P_f = 4331$ N, (+) $P_f = 5617$ N, (●) $P_f = 6420$ N; (b) LUCF prestressing 10 kN, fracturing at −196°C: (●) $P_f = 0$ N, (×) $P_f = 765$ N, (■) $P_f = 2105$ N, (▲) $P_f = 3636$ N, (♦) $P_f = 5167$ N, (+) $P_f = 6699$ N, (●) $P_f = 7656$ N.

average value of fracture load for the CF specimens. The values of the crack opening displacement and the peak residual compressive stress calculated at the beginning of the fracture steps are also listed in Table 3. Table 4 is for the case at −130°C at an applied load of 9500 N, which is also the average value of fracture load for the CF specimens at −130°C. Measured values of the local fracture stress σ_f are also listed. Figs. 12 and 13 illustrate respectively the results shown in Tables 3 and 4.

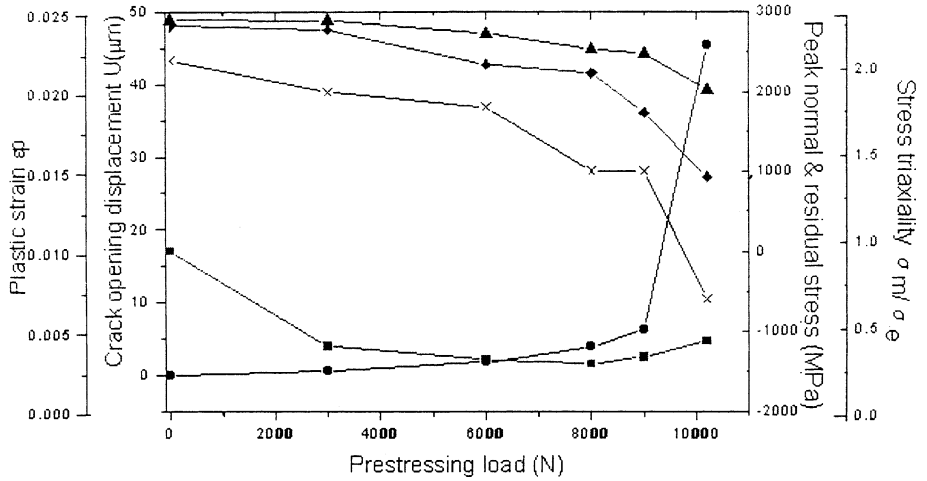

Fig. 12. Fracture-related mechanical parameters produced by LUCF cycle with various prestressing load, fracturing step at −196°C: (▲) peak normal stress ahead of precrack tip produced by 5000 N load at −196°C, (♦) peak stress triaxiality ahead of precrack tip produced by 5000 N load at −196°C, (×) plastic strain, (●) crack opening displacement, (■) residual compressive stress.

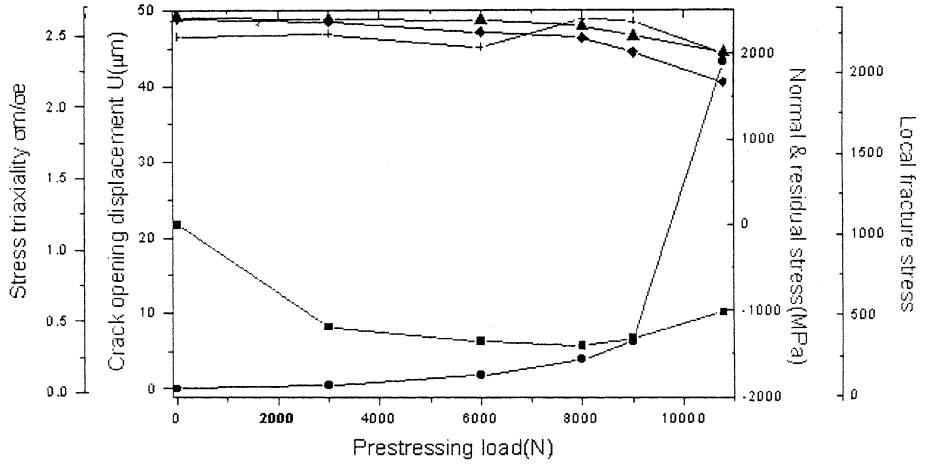

Fig. 13. Fracture-related mechanical parameters produced by LUCF cycle with various prestressing load, fracturing step at −130°C: (▲) peak normal stress ahead of precrack tip produced by 5000 N load at −130°C, (♦) peak stress triaxiality ahead of precrack tip produced by 5000 N load at −130°C, (+) local fracture stress, (●) crack opening displacement, (■) residual compressive stress.

From Table 3 and Fig. 12 it is found that the peak normal stress σ_{peak} produced by a fracturing load of 5000 N at −196°C decreases with increase of prestressing load at room temperature. For CF specimens without prestressing, a 5000 N applied load results in a σ_{peak} of 2900 MPa and the fracture of the specimens. With increasing prestressing load P_0 to over 8000 N σ_{peak} apparently decreases. Comparing with Fig. 6(c) the apparent toughness of the specimen is distinctly improved at the same range of P_0. From the criterion of normal stress exceeding the local fracture stress for cleavage it is reasonable to attribute the toughness improvement to the decrease of σ_{peak} by prestressing. By further comparing the appearance of the various curves in Fig. 12, those of the stress triaxiality σ_m/σ_e and plastic strain ε_p present a similar decreasing trend

to that of σ_{peak}. Because the intensification of normal stress results from the effects of σ_m/σ_e and ε_p ahead of a precrack, the decrease of σ_{peak} is obviously caused by decreasing of these two parameters. The crack opening displacement U caused by prestressing load shows a growing trend and a notable increase at $P_0 = 9000$ N where all parameters including apparent toughness, σ_{peak}, σ_m/σ_e, and ε_p show corresponding apparent changes.

From the observed phenomena and the inherent relationship between σ_m/σ_e, ε_p and crack tip radius it is concluded that the crack blunting caused by prestressing is a fundamental factor for improving the apparent fracture toughness. Due to the blunting of the precrack tip, the stress triaxiality and plastic strain produced by the fracture load ahead of the blunted crack are relaxed. Accordingly the normal stress intensified by the stress triaxiality and strain hardening is lower and the cleavage occurs at a higher fracture load.

In the case of fracture loading at −130°C (Table 4 and Fig. 13), the variations of mechanical parameters follow the same general trend, but the effects of crack tip blunting are much weaker. Correspondingly the improvement of apparent toughness by WPS is much less comparing to the case of fracturing at −196°C (compare Figs. 6 and 7).

In LCUF cycles the unloading step is carried out at low temperature, the blunted crack tips are recovered (sharpened) by a lower degree than those in LUCF cycle. Correspondingly, the values of σ_m/σ_e, ε_p, and σ_{peak} produced by following fracturing loading are lower. Therefore the LCUF cycles offer stable and high toughness values compared with those produced by LUCF (Figs. 6 and 7).

From experimental results observed in specimens which have been torn before the fracturing step, it seems that short micro-cracks (20–30 μm) produced by WPS have not appreciable effect on the general trend of the experimental data.

4.2. Effects of residual compressive stress

From Figs. 12 and 13 it is found that the trends of the variation in the residual compressive stresses produced by prestressing loading and unloading are not consistent with those of normal tensile stress produced by fracture loading. In the region of over about 9000 N prestressing, the σ_{peak} decreases apparently however at a condition that the residual compressive stress reduces. It means that the apparent reduction of σ_{peak} resulting from the effects of WPS is not caused by an increase of residual compressive stress.

In order to clarify the effects of residual compressive stress, calculations are carried out for CF specimen with similar crack tip radius, which has been produced in specimen experienced WPS loading and unloading. For both specimens, calculations start from a similar crack tip radius of around 15 μm. However in the former there are not residual compressive stresses, which exist in the latter. The results of the calculations are presented in Table 5. Here the effect of the blunting crack tip is excluded by using a similar starting crack tip radius for specimens with and without WPS.

From Table 5 it is revealed that the residual compressive stress produced by prestressing loading and unloading leads to an appreciable effect on reducing the normal tensile stress produced by fracture loading at −196°C. This effect is caused by reducing the stress triaxiality σ_m/σ_e and the current yield stress σ_y. (Due to the Bauschinger effect the current yield stress at the fracture step is limited by that reached at the unloading step.) But the effect resulting from residual compressive stress is lower, compared to that caused by crack tip blunting. In the case of fracture at −130°C, the effect of residual compressive stress is even lower and can be ignored.

In the LUfLUCF cycles the specimens are loaded first then unloaded and reloaded at opposite direction to return the crack tip radii to almost the original values, then cooled and fractured. In this case the effect of crack tip blunting is removed but the residual stress is tensile rather than compressive as in the above cases.

Table 5
Results of calculations for specimens with and without residual compressive stress

	Applied fracturing loading of 7760 N at −196°C		Applied fracturing loading of 11 850 N at −130°C	
	$P_0 = 0$ with residual compressive stress = 0	$P_0 = 9699$ N with residual compressive stress ≈ −1000 MPa	$P_0 = 0$ with residual compressive stress = 0	$P_0 = 9699$ N with residual compressive stress ≈ −1000 MPa
Starting crack radius (μm)	15	Around 15	15	Around 15
Final crack radius (μm)	19.68	20.56	26.74	36
σ_{peak} (MPa)	2782	2596	2285	2309
σ_m/σ_e	2.167	1.8	2.493	2.382
ε_p	0.013	0.015	0.016	0.0196
σ_y (MPa)	1005	850	704	500
X_f (μm)	67	47	93	67

P_0 is the warm prestressing load, σ_{peak} the normal tensile stress, σ_m/σ_e the stress triaxiality, ε_p the plastic strain, σ_y the current yield stress, $\sigma_y X_f$ the distance from cleavage origin to blunted crack tip.

As shown by Fig. 3, the values of apparent toughness of specimens experienced LUfLUCF cycles are appreciably lower than those of CF specimens.

It is concluded that contrary to the case of notch specimens [12], in precracked specimens the residual compressive stress plays only a secondary role for improving the apparent toughness by WPS. However, a residual tensile stress appreciably decreases the apparent toughness.

4.3. Effects of LCF cycle

The apparent toughness value presented in specimens experiencing LCF cycles is always higher than that of prestressing loading value presented in toughness-related parameters, K_1, δ_1 or P_0 (Figs. 6 and 7). This can be explained by following events:

1. During the cooling step the applied load almost keeps constant, no additive stress exerts.
2. For cleavage cracking at low temperature, a new crack nucleus should be nucleated by a further increased load even though the current load is higher than that for directly cleaving at the same temperature.

Thus the mechanism of the improving apparent toughness by the LCF cycle is essentially different from that by LUCF and LCUF cycles.

4.4. Different behaviors of WPS effects in specimens fractured at −196°C and −130°C

The WPS cycles show appreciably stronger effects in specimens fractured at −196°C than in those fractured at −130°C (compare Figs. 6, and 7, 12 and 13). The reason can be explained as follows: For a sharp crack (tip radius less than 0.1 μm) the normal tensile stress ahead of it is intensified rapidly with applied load. At an applied load of about $0.2P_{gy}$ σ_{peak} reaches its 'saturated' value (as schematically shown in Fig. 14(a)). For a blunted notch specimen it is reached much later at about $0.9P_{gy}$ (as schematically shown in Fig. 14(b)). For specimens fractured at −196°C the fracture load P_f is much lower than the P_{gy}, ($P_f/P_{gy} = 0.3$–0.6). In case of CF cycle with a sharp crack specimen at $P_f/P_{gy} = 0.3$–0.6 the normal tensile stress has reached a high 'saturated' value but in LUCF cycle the sharp crack is blunted to a notch, σ_{peak}, at same applied load, is much lower than its 'saturated' value. Therefore in case of fracture at −196°C the

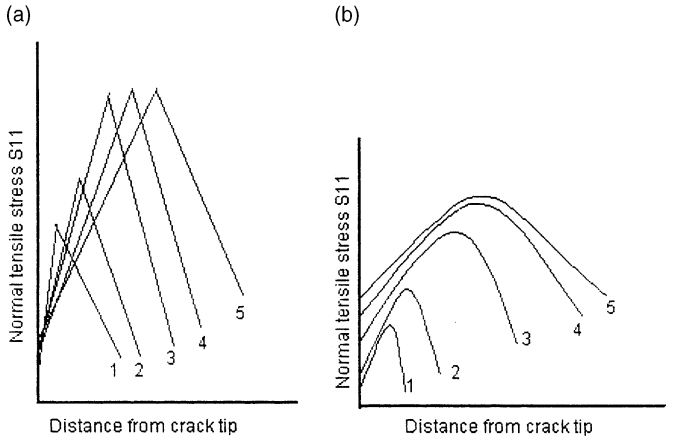

Fig. 14. Schematics of normal tensile stress distributions: (a) in front of a sharp crack – 1. $P/P_y = 0.05$, 2. $P/P_y = 0.1$, 3. $P/P_y = 0.2$, 4, 5. $P/P_y > 0.2$ and (b) in front of a blunted notch 1. $P/P_y = 0.35$, 2. $P/P_y = 0.45$, 3. $P/P_y = 0.67$, 4. $P/P_y = 0.95$, 5. $P/P_y = 1.05$. P is the applied load, P_y the general yield load.

WPS benefits the apparent toughness not only through decreasing the 'saturated' normal tensile stress by blunting but also through decreasing the level of 'saturation' of the normal tensile stress.

In case of fracture at −130°C P_f is close to P_{gy}, $P_f/P_{gy} = 0.9$. Even in a notched specimen σ_{peak} has reached its 'saturated' value. Therefore the WPS benefit the apparent toughness only through decreasing the 'saturated' normal tensile stress by blunting and its effect is much lower than in case of fracture at −196°C.

5. Conclusion

By investigating the variations of apparent toughness measured at low temperature in precracked HSLA steel specimens experiencing various cycles of WPS and comprehensive FEM calculations, the mechanism for the effects of WPS can be summarized as follows:

(1) The local fracture stress σ_f remains almost constant after WPS at various levels. The real toughness of steel is almost unmodified by WPS.

(2) The appreciable effects improving the apparent toughness due to WPS present in specimens experiencing WPS loads close to the general yield load.

(3) The crack blunting caused by WPS is a fundamental factor for improving the apparent fracture toughness of precracked specimens by reducing the stress triaxiality and plastic strain produced in the fracture step.

(4) In precracked specimens the residual compressive stress plays only a secondary role for improving the apparent toughness by WPS. However, a residual tensile stress appreciably decreases the apparent toughness.

(5) The WPS cycles show appreciably stronger effects in specimens fractured at −196°C than in those fractured at −130°C, due to the normal tensile stresses at theses two temperatures developing into different levels of saturation in prestress-blunted notch specimens.

(6) The mechanism of improving apparent toughness by the LCF cycle is essentially different from that by LUCF and LCUF cycles. A further increase in applied load is necessary for cleavage after loading and

cooling steps even though the prestressing load is higher than that needed for direct cleavage at low temperature.

Acknowledgements

This work was financially supported by the National Natural Sciences Foundation of China (5987101) and Gansu Province (ZS981-A22-053-C). Authors like to express their gratitude to Mr. Li Zheng and Mr. Wang Jung Gang for preparing figures.

References

[1] Nichols RW. Br Welding J 1968;15:21–42.
[2] Harrison TC, Fearnehough GD. J Basic Engng 1972. p.373–376.
[3] Chell GG, Haigh JR, Vitek V. Inter J Fract 1981;17:61–81.
[4] Curry DA. Inter J Fract 1983;22:145–59.
[5] Ritchie RO, Knott JF, Rice JR. J Mech Phy Solids 1973;21:395–410.
[6] Reed PAS, Knott JF. Adv Res Fract Proc of ICF7. vol.4. New York: Pergamon Press; 1989. p. 2583–93.
[7] Reed PAS, Knott JF. Fatigue Fract Engng Mater Strict 1996;19(4):485–500.
[8] Reed PAS, Knott JF. Fatigue Fract Engng Mater Strict 1996;19(4):501–13.
[9] Timofeev BT, Smirnov VI. Int J Pres Ves and Piping 1995;63:135–42.
[10] Stoeckl H, Boeschen R, Schmitt W, Varfolomeyev I, Chen JH. Engng Fract Mech 2000;67:119–37.
[11] Shum DKM. in: F. Erdogan, editor. Fracture Mechanics: 25th Volume, ASTM STP 1220, 1995, p. 686–704.
[12] Chen JH, Dong ZQ, Wang GZ, 2000, submitted to Metall Trans.